LEVEL

A061224

(12) SC

17

OPTICAL—MICROWAVE INTERACTIONS IN SEMICONDUCTOR DEVICES

L. Figueroa, C. Slayman, and H. W. Yen

Hughes Research Laboratories

3011 Malibu Canyon Road

Malibu, CA 90265

April 1979

DDC
RECEIVED
MAY 7 1979
C

Approved for public release; distribution unlimited.

79 05 07 004
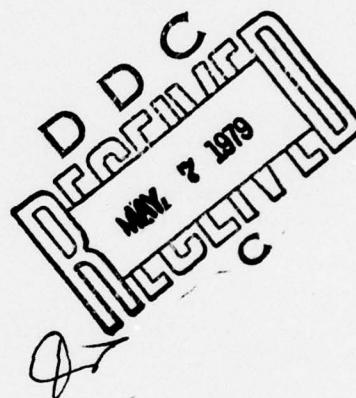
REPORT DOCUMENTATION PAGE		READ INSTRUCTIONS BEFORE COMPLETING FORM
1. REPORT NUMBER	2. GOVT ACCESSION NO.	3. RECIPIENT'S CATALOG NUMBER
4. TITLE (and Subtitle) OPTICAL-MICROWAVE INTERACTIONS IN SEMICONDUCTOR DEVICES.		5. TYPE OF REPORT & PERIOD COVERED Quarterly Report. no. 3, 1 Jan — 31 Mar 79.
		6. PERFORMING ORG. REPORT NUMBER
7. AUTHOR(s) L. Figueroa, C. Slayman H.W. Yen		8. CONTRACT OR GRANT NUMBER(s) N00173-78-C-0192
9. PERFORMING ORGANIZATION NAME AND ADDRESS Hughes Research Laboratories 3011 Malibu Canyon Road Malibu, CA 90265		10. PROGRAM ELEMENT, PROJECT, TASK AREA & WORK UNIT NUMBERS
11. CONTROLLING OFFICE NAME AND ADDRESS Defense Advanced Research Projects Agency 1400 Wilson Boulevard Arlington, VA 22209		12. REPORT DATE April 79
		13. NUMBER OF PAGES 37
14. MONITORING AGENCY NAME & ADDRESS(if different from Controlling Office) Naval Research Laboratory 4555 Overlook Ave., S.W. 38 p. Washington, DC 20375		15. SECURITY CLASS. (of this report) UNCLASSIFIED
		15a. DECLASSIFICATION DOWNGRADING SCHEDULE

16. DISTRIBUTION STATEMENT (of this Report)

Approved for public release; distribution unlimited.

17. DISTRIBUTION STATEMENT (of the abstract entered in Block 20, if different from Report)

18. SUPPLEMENTARY NOTES

19. KEY WORDS (Continue on reverse side if necessary and identify by block number)

Mode-locking of injection lasers, External resonators, Optical fiber resonators, GaAs FETs, High-speed optical detectors

approximately

20. ABSTRACT (Continue on reverse side if necessary and identify by block number)

The results of an extensive experimental study of mode locking in semiconductor lasers with different external-cavity configurations are described. The generation of GaAs laser pulses less than 200 psec wide at ~3-GHz repetition rates was achieved by operating the laser in a 5-cm-long external cavity. The presence of a strong resonance at low frequencies in the laser actually aided the generation of short pulses. A novel external-cavity configuration using a piece of optical fiber is →

DD FORM 1473 EDITION OF 1 NOV 65 IS OBSOLETE

172 600

cont.

also described. Modulation frequencies as high as 4.26 GHz were obtained for lasers biased only slightly above threshold, and optical pulses as narrow as 200 psec were generated using this technique.

A theoretical study of the response of GaAs FETs under optical illumination was presented. For a strong photo-transistor effect to occur in an FET requires that the region of active channel under the gate electrode be illuminated. A modified FET design suitable for this purpose is proposed and analyzed.

TABLE OF CONTENTS

LIST OF ILLUSTRATIONS

4

PREFACE

The following personnel contributed to the research work reported here: L. Figueroa, C. Slayman, H.W. Yen, M.K. Barnoski, A. Yariv (consultant), and D.F. Lewis.

SECTION 1

INTRODUCTION AND SUMMARY

In this program we are concerned with both the modulation of optical beams at microwave frequencies and the use of optical signals to control microwave semiconductor devices to achieve various functions such as injection locking and switching of oscillators, mixing and detection of microwave modulated optical signals, etc. To achieve these goals, two important issues must be resolved: how to generate microwave modulated optical signals from semiconductor lasers, and how to couple light efficiently into microwave devices.

Semiconductor laser output can be modulated either by an external modulator or by direct current modulation. External modulation has the advantage that the laser retains cw operation and therefore that its output spectrum does not vary with time and the modulation speed is not limited by the frequency response of the laser. In contrast, direct modulation has a practical frequency limit of no more than 10 GHz. However, its simplicity makes it very attractive. So far in this program, we have concentrated our efforts on the direct-modulation approach. Both sinusoidal modulation and mode locking (short-pulse generation) are being pursued.

During the past quarter, we carried out an extensive experimental study of mode locking in semiconductor lasers with two different external-cavity configurations.

We have achieved the generation of GaAs laser pulses less than 200 psec wide at approximately 3 GHz repetition rates. The presence of a strong resonance at low frequencies (100 to 200 MHz) in the laser actually aids the generation of short pulses. However, the presence of the resonance produces significant noise, which may be detrimental to proper laser operation.

When a piece of optical fiber is used as part of the laser resonator, a narrow-band microwave resonance corresponding to the inverse of the photon round-trip time in the resonator is generated. We have achieved enhanced laser modulation over this narrow band. Modulation frequencies

7

as high as 4.26 GHz have been obtained for lasers biased only slightly above threshold, and optical pulses as narrow as 200 psec have also been generated using this technique.

A theoretical study of the response of GaAs FETs under optical illumination was carried out. We found that, with intense optical signal, it is possible to obtain significant gate depletion-width change in an FET. Thus, phototransistor action can take place in an FET if it is designed so that the region under the gate electrode can also be illuminated. A modified FET design is proposed, and its feasibility is discussed. The new device is similar to a Burrus LED in structure. Part of the substrate is etched away to allow the optical beam to cover the entire active channel region of the transistor. The modifications to the device are believed to only negligibly degrade the FET's characteristics.

SECTION 2

MODE-LOCKING OF INJECTION LASERS

In the last report, we discussed the characteristics of two different external-cavity configurations and their effect on injection laser mode locking. We found that the three-mirror cavity has a higher Q and should be more effective for mode-locking purposes. This section describes theoretical and experimental studies of GaAs stripe geometry lasers operating in a three-mirror cavity. Some preliminary results on the lasing properties of a novel external resonator using optical fiber are also presented.

A. EFFECTS OF AN EXTERNAL MIRROR ON INJECTION LASER OUTPUT

A schematic of the external cavity discussed in this section is shown in Figure 1. The use of an external cavity can reduce the laser threshold current caused by the increased reflectivity from the external mirror. To study this effect quantitatively requires determining the effective reflectivity of the composite laser resonator. The relation between laser mode gain and threshold current is[1]

$$G_{th} = \beta J_{th} = \alpha + \left(\frac{1}{2\ell}\right) \ln \left(\frac{1}{RR_{eff}}\right), \qquad (1)$$

where G_{th} is the threshold mode gain, β is the gain coefficient, J_{th} is the threshold current density, α is the internal loss coefficient due to free carrier absorption and scattering, ℓ is the length of the laser diode, R is the reflectivity of the laser cleaved facet, and R_{eff} is defined as the fraction of light reflected back into the laser from the external mirror and the diode facet combination.

Define a coupling parameter k as the ratio of threshold current densities with and without external mirror such that

$$k = \frac{\alpha + \left(\frac{1}{2\ell}\right) \ln \left(\frac{1}{RR_{eff}}\right)}{\alpha + \left(\frac{1}{\ell}\right) \ln \left(\frac{1}{R}\right)}. \qquad (2)$$

9

Using the following typical values, $\ell = 300$ µm, $\alpha = 20$ cm^{-1}, $R = 0.3$, and $R_{eff} = 1$, the minimum value of k can be calculated to be $k_{min} = 0.67$. R_{eff} for a laser with external mirror can be calculated to be

$$R_{eff} = \frac{R + 2\sqrt{R}\ \sqrt{R_m}\ \cos 2\delta + R_m}{1 + 2\sqrt{R}\ \sqrt{R_m}\ \cos 2\delta + RR_m} \quad ,$$

where 2δ is the round-trip phase delay of wave propagation between the laser end face and the external mirror, and R_m is the reflectivity of the mirror. The value of R_{eff} varies between a maximum of

$$R_{eff}^{max} = \frac{(\sqrt{R} + \sqrt{R_m})^2}{(1 + \sqrt{R}\ \sqrt{R_m})^2} \tag{3}$$

and a minimum of

$$R_{eff}^{min} = \frac{(\sqrt{R} - \sqrt{R_m})^2}{(1 - \sqrt{R}\ \sqrt{R_m})^2} \quad . \tag{4}$$

7963-1
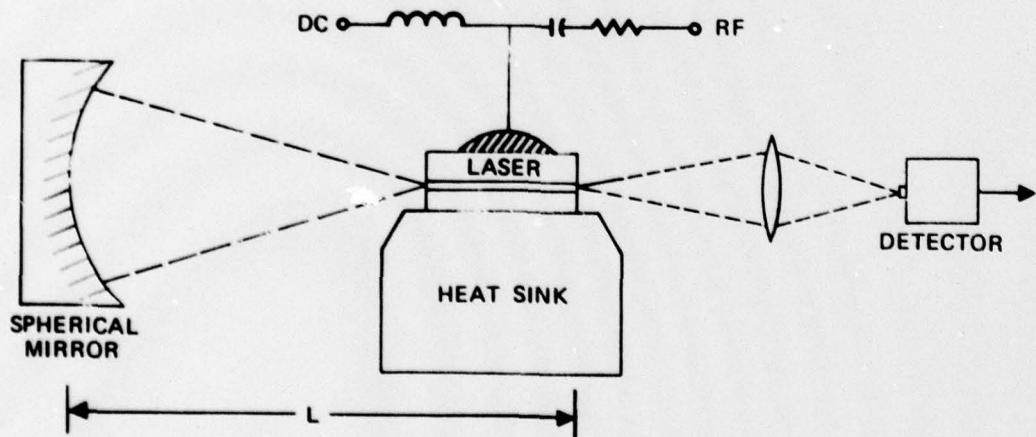
Figure 1. Schematic of injection laser mode-locking experimental setup.

10

Figure 2 shows a plot of measured light output versus current input for an injection laser (Laser Diode LCW-10) with and without the external mirror. The graph shows that k is approximately 0.8 for this particular laser and external resonator. To compare this value with the theoretical, assume that all the losses in the external cavity are due to diffraction losses in the plane perpendicular to the laser junction plane. The external mirror, with diameter $D = 2.54$ cm, is positioned at a distance $L = 5$ cm from the laser diode. If the full beam divergence angle for the diode is taken to be $\Delta\theta = 50°$, and the reflectivity of the mirror itself is taken to be unity, then the fraction of light reflected from the external mirror is

$$R' \approx \frac{D}{2L \, \tan(\Delta\theta/2)} \, . \tag{5}$$

Thus, R' is the effective reflectivity of the external mirror. Combining the above information with Eqs. 3 and 5 yields $R' = 0.545$ and $R_{eff}^{max} = 0.845$. Substituting these values into Eq. 2 yields $k = 0.71$. The calculated value is smaller than the measured value of 0.8, which indicates that the effective mirror reflectivity as given by Eq. 5 is too optimistic.

To obtain a smaller k, the beam divergence of the laser must be reduced or the diameter of the external mirror increased. However, the diameter of the external mirror cannot be increased arbitrarily for small radii of curvature ($r < 5$ cm). Therefore, the only alternative is to reduce the beam divergence of the laser. This can be done by using a structure such as a channeled-substrate-planar (CSP) laser[2] or large-optical-cavity (LOC) laser.[3,4]

B. CHARACTERISTICS OF INJECTION LASERS WITH AN EXTERNAL FIBER RESONATOR

During the mode-locking study, we developed a new form of external resonator. This resonator consists of a piece of graded index fiber with both ends cleaved. One end of the fiber is coated with a thin
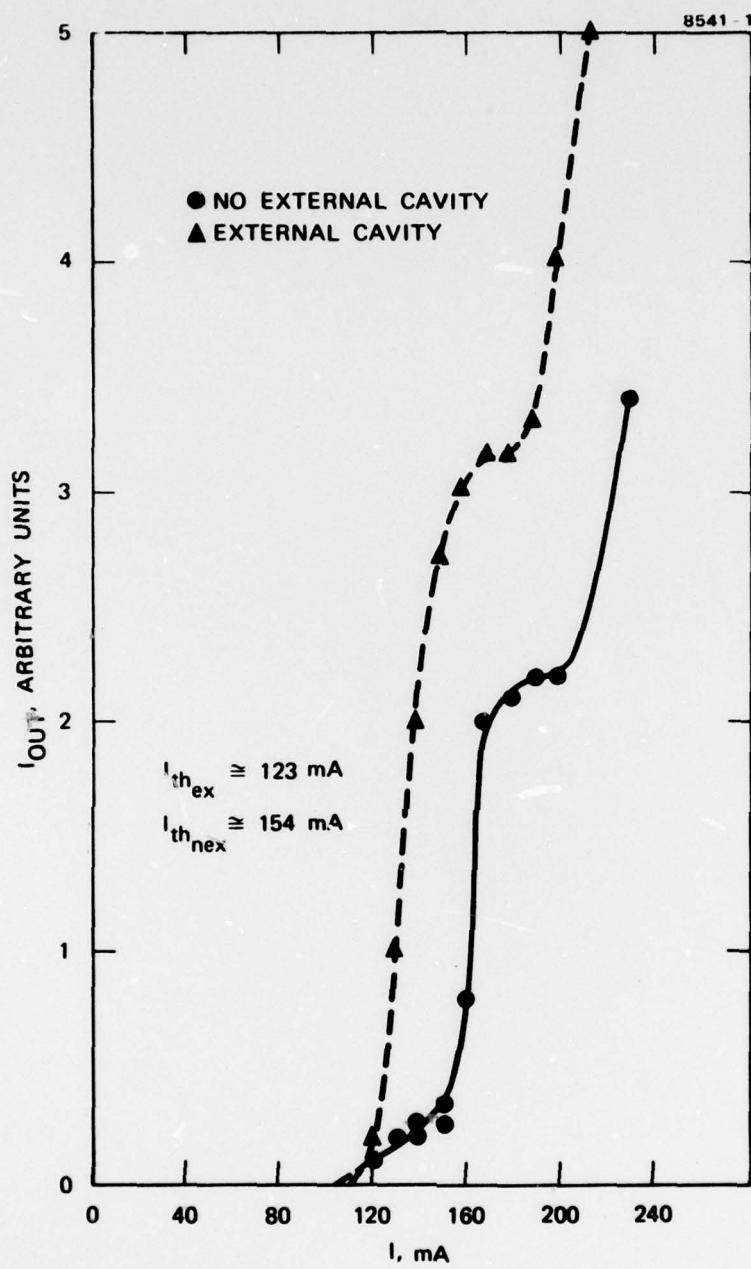
Figure 2. Light output versus current of a laser diode with and without an external mirror.

12

layer of gold to form a reflector. A spherical lens is formed on the other end to facilitate optical coupling between the laser and the fiber. Figure 3 shows the actual fiber end with spherical lens formed. We have found that it is much easier to align a fiber resonator than an external mirror resonator.

Experiments were carried out using RCA injection lasers. A plot of light output versus current is shown in Figure 4. Threshold current was reduced 10% with the laser in a fiber resonator, which resulted in a value of $k \sim 0.9$, or $R_{eff} = 0.43$.

There are several possible sources of loss in the fiber resonator; the most significant ones are

- Reflection loss at the fiber lens

- Coupling loss between the laser and the fiber

- Polarization conversion in the fiber.

Assuming normal incidence, the reflection loss at the fiber lens is given by

$$R_f = \left(\frac{n_c - 1}{n_c + 1} \right)^2 \, ,$$

where n_c is the index of refraction of the fiber core. For an n_c of 1.5, R is only about 4%. The coupling loss can be estimated from the fiber acceptance angle, the laser divergence angle, and the fiber lens focal distance. The fiber used in the experiment had a numerical aperture of ~ 0.14 without lens. The diameter of the fiber core was 65 μm, and the radius of curvature of the lens was 110 μm as measured from Figure 3. The new half-cone acceptance angle of the fiber with lens can be calculated[4] to be $\theta_{1/2} = 18°$. The coupling efficiency η is then given by the ratio of the integrals as:

$$\eta = \frac{\int_0^{\theta_{1/2}} I(\theta) \sin \theta \, d\theta}{\int_0^{\pi/2} I(\theta) \sin \theta \, d\theta} \, , \tag{4}$$

13

where the fiber is assumed to couple all the light in the lateral direction since the laser beam divergence is smaller in that dimension. The far field distribution of the laser can be approximated by

$$
I(\theta) = \begin{cases} I_o \cos(2.4\theta) & \text{for} \quad |\theta| < 37° \\ \\ 0 & \text{for} \quad |\theta| > 37° \end{cases} \quad . \tag{5}
$$

Using Eqs. 4 and 5, we find $\eta = 0.44$. For the same fiber without the lens, we find that $\eta \sim 0.11$. Therefore, the lens improves the coupling efficiency significantly.

Another effect that must be considered is the polarization conversion inside the fiber. The output of an injection laser is primarily polarized along the junction plane (TE polarization). Thus, the polarization conversion in the fiber effectively reduces the efficiency of light coupling back into the laser. For a propagation length of 50 cm in a step-index multimode fiber, the polarization of the incident wave is completely mixed. For a single-mode fiber, the fiber length required for depolarization is much larger (>300 m). We believe the depolarization length for a graded index fiber is similar to that of a step-index fiber. If we use a linear relation between the precentage of polarization conversion and the distance traveled, then, for a fiber resonator of length L/2 (in cm), the fraction of light coupled back into the laser is

$$
\gamma = \begin{cases} 1 - 0.5 \left(\dfrac{L}{50}\right) & \text{for} \quad L \leq 50 \text{ cm} \\ \\ 0.5 & \text{for} \quad L \geq 50 \text{ cm} \end{cases} \quad .
$$

14

100 μm
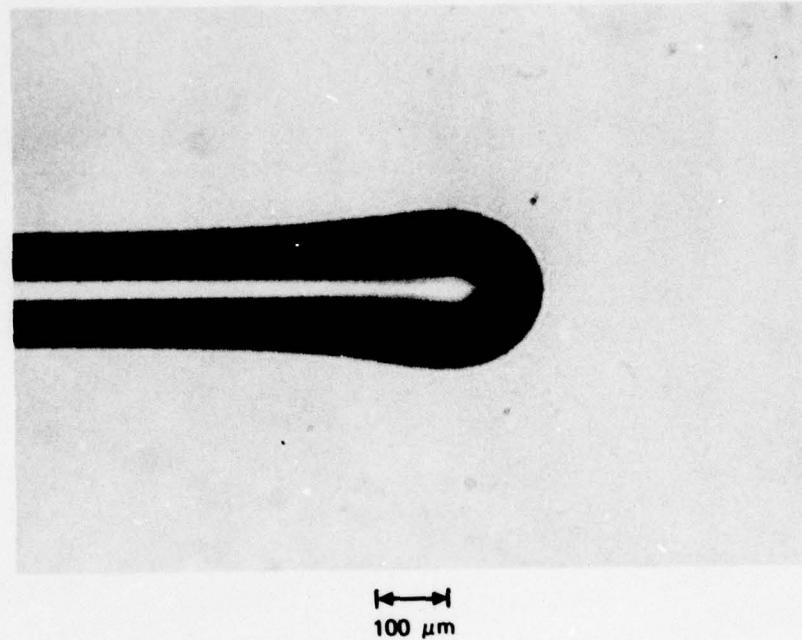
Figure 3. Fiber resonator with spherical lens on one
end.
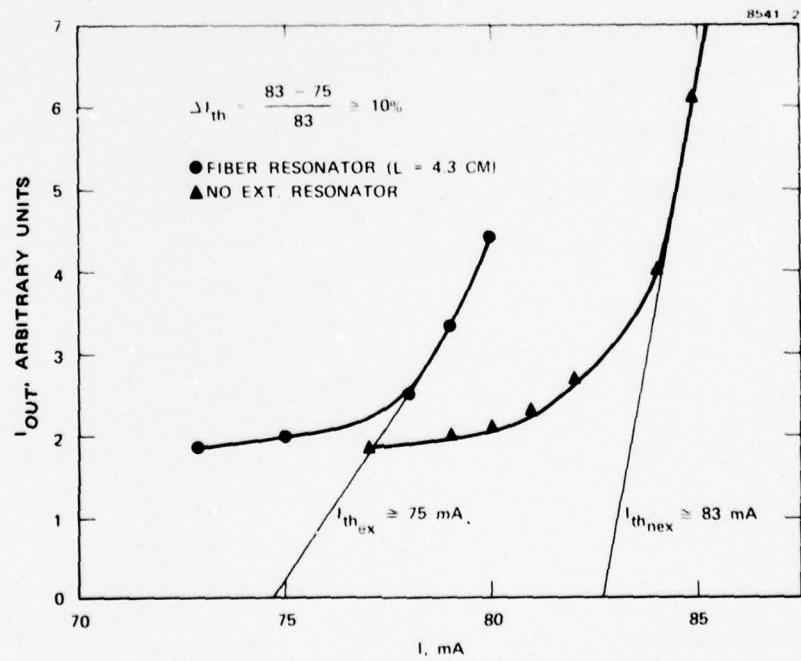
Figure 4. Light output versus current of a laser
diode with fiber external resonator.

15

For L = 8.6 cm (fiber length 4.3 cm), γ is 0.91.

The effective reflectivity of the fiber resonator can, therefore, be obtained by combining the various loss mechanisms to give

$$R_{eff} = \eta(1 - R_f)\gamma R_e \quad ,$$

where R_e is the reflectivity of the coated fiber end. Thus, the estimated effective reflectivity of our external fiber resonator is R_{eff} = 0.39. The measured value is 0.43. The discrepancy lies mostly in the estimation of the laser-to-fiber coupling efficiency.

C.   INJECTION LASER OUTPUT WITH EXTERNAL RESONATOR

The frequency response of an injection laser under direct current modulation has been calculated and measured.[5,6] Semiconductor lasers exhibit a sharp resonance in their small-signal frequency response due to the coupling between photons and injected carriers. The resonance peak frequency f_r coincides with the laser relaxation oscillation frequency and is given by

$$f_r = \frac{1}{2\pi(\tau_p\tau_s)^{1/2}}\left(\frac{I}{I_{th}} - 1\right)^{1/2} \quad , \tag{6}$$

where τ_s is the electron spontaneous liftime, τ_p is the photon cavity lifetime, and I/I_{th} is the ratio of the driving current to the threshold current. The effect of an external cavity is to increase the cavity lifetime since τ_p is proportional to the total optical cavity length. This in turn decreases the resonance frequency f_r (as is evident from Eq. 6). The frequency response of injection lasers in an external cavity has been calculated by Broom et al.[7] They found that only a small amount of feedback from the external cavity is required to suppress the relaxation oscillation peak. They also observed that, when f_c (inverse of the cavity round-trip transit time) is a harmonic of the relaxation oscillation frequency f_r, there is a resonance in the laser modulation response at f_r. In general, the resonance only occurs over a small range

16

of current and external-cavity coupling coefficients. In our experiment, we obtained similar results to those of Broom et al. in some of the lasers tested, while in some other lasers we observed quite different behaviors. Some of our experimental results are presented and interpreted below.

The experimental arrangement is similar to that shown in Figure 1. A strip-line bias circuit was used to supply the laser with dc bias current and rf modulation signal. The semiconductor laser was placed near the focal point of the spherical mirror, and final alignment was carried out using PZT-controlled micrometers. The measured threshold current of the laser (Laser Diode LCW-10) was $\sim$150 mA with the external mirror aligned and $\sim$165 mA without the external cavity. The laser output was detected by a silicon avalanche photodiode and monitored with either a microwave spectrum analyzer or a sampling scope. The total external cavity length was 5.24 cm, which gives a cavity round trip frequency of f_c = 2.86 GHz. Figure 5 shows the microwave spectrum of the laser output. In Figure 5(a), the laser was driven at 1.43 GHz, and the modulated light output was resonantly enhanced at this frequency. Along with the main peak at 1.43 GHz, there are two sidebands at roughly (1.43 ± 0.1) GHz. Note that the resonance observed there corresponds to one-half of the cavity round-trip frequency f_c. A possible explanation is that there are several transverse modes in the laser and that the round-trip cavity resonance involves coupling between these modes. The end result of this process would be to double the transit time of the resonator. Figure 5(b) shows the low-frequency resonance ($\sim$100 MHz) spectrum of the laser output. We believe that the sidebands observed in Figure 5(a) are a result of the interaction between the cavity transit frequency and this low-frequency resonance. We verified the existence of this phenomenon by detuning the external cavity to show that the presence of a low-frequency resonance affected the sidebands at high-frequency resonance. The low-frequency resonance is also related to the laser's self-pulsation. The amplitude noise generated in laser output can actually be observed on the oscilloscope. Figure 6 shows the

17

8541–5
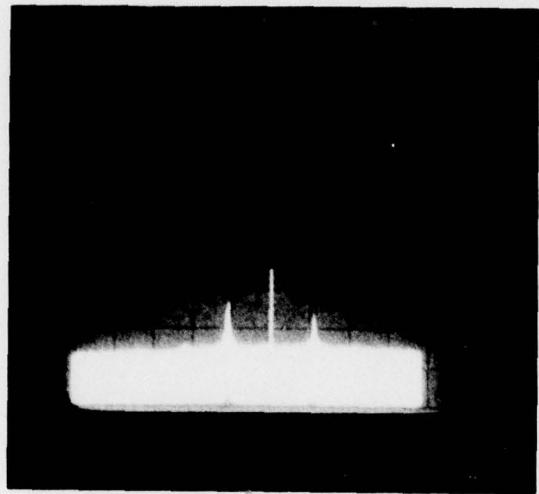
(a) Laser driven at 1.43 GHz.

(b) Low-frequency resonance
of the laser.
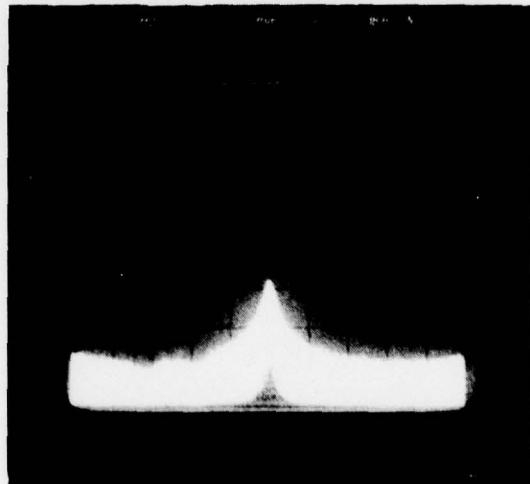
Figure 5. Spectrum analyzer display of laser output.

18

8541-3
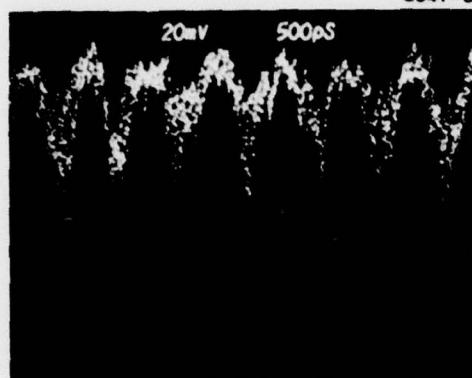
(a) 500 psec/div.
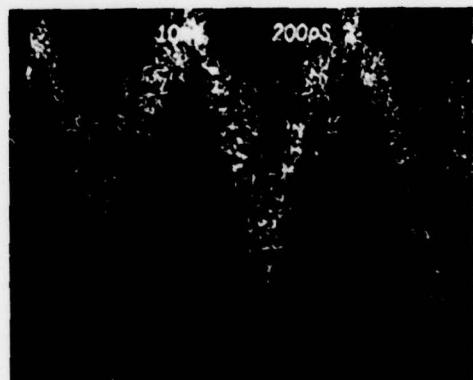
(b) 200 psec/div.

Figure 6. Temporal display of laser output pulse shape (negative going
pulses).

19

temporal display of the laser output driven at 1.43 GHz. The output
is pulse-like modulation. There seem to be many substructures within
each pulse. Since the risetime of the detector used was about 130 psec,
any fast varying signal will not be faithfully recorded. We believe
that the presence of the low-frequency resonance actually aids the gen-
eration of sharper pulses; this is evident in Figure 7. Figure 7(a)
shows the laser temporal output when the low-frequency response does not
exist. The output modulation resembles sinusoidal variations. How-
ever, a pronounced spiking is observed when the low-frequency resonance
is present, as shown in Figure 7(b). The sharpness of the pulsation
seems to be related to the magnitude of the low-frequency resonance,
perhaps as a result of the interaction by which the laser is mode locked
in both the first- and second-order* process.[8-10] The dispersion in the
laser medium leads to unequal longitudinal mode spacings. When the
laser resonance is excited through nonlinear mode-mixing in the active
laser medium, second-order locking of the longitudinal modes can occur.
This locking produces a self-induced pulsation of the laser intensity at
a frequency two orders of magnitude lower than the longitudinal mode
separation. Because of material dispersion, the input rf power is able
to couple relatively few modes of the laser through first-order mode
locking. The remaining modes, however, can be locked through the second-
order process. Paoli and Ripper[11] have suggested that a strong locking
action may occur if

$$mf_L = nf_c \quad ,$$

---

*In a first-order mode-locked laser, the difference between the fre-
quencies f_i and f_{i+1} of two adjacent longitudinal modes is a constant
equal to the repetition rate of the resulting pulses. However, in a
semiconductor laser the high dispersion can lead to a phase locking of
the laser modes in groups of three or four such that the difference
$(f_i - f_{i-j}) - (f_{i+j+k} - f_{i+k})$ is constant, independent of the mode
number i for fixed j and k. This type of locking is refereed to as
second-order mode-locking since it involves the difference between the
mode spacings.

20

where m and n are integers, f_L is the second-order locking resonance frequency, and f_c is the cavity round-trip frequency. The laser used in our experiment exhibits strong self-pulsation at 180 MHz without an external cavity. The pulse width of the laser when modulated at 1.43 GHz was ∿500 psec. Therefore, the effect of the external resonator was to produce the double-locking action and narrow the pulse width to less than 200 psec.

We have also used a different alignment of the cavity; it yielded a higher output power and a higher resonance frequency at 2.83 GHz (roughly the transit time frequency). Figure 8(a) displays the micro-wave spectrum of the realigned laser output without driving signal. Note the relatively sharp resonance at 2.831 GHz. Figure 8(b) shows the narrowing of the resonance when an external signal is applied to the laser. Again there are sidebands on each side of 2.831 GHz, similar to those shown in Figure 5 but smaller in magnitude. Figure 9 gives the temporal display of the laser output, which shows what appears to be a pulsation in light output. However, the width of the pulses is much larger than that obtained previously. This gives further

8541-4

(a) No sidebands present

(b) Sidebands present
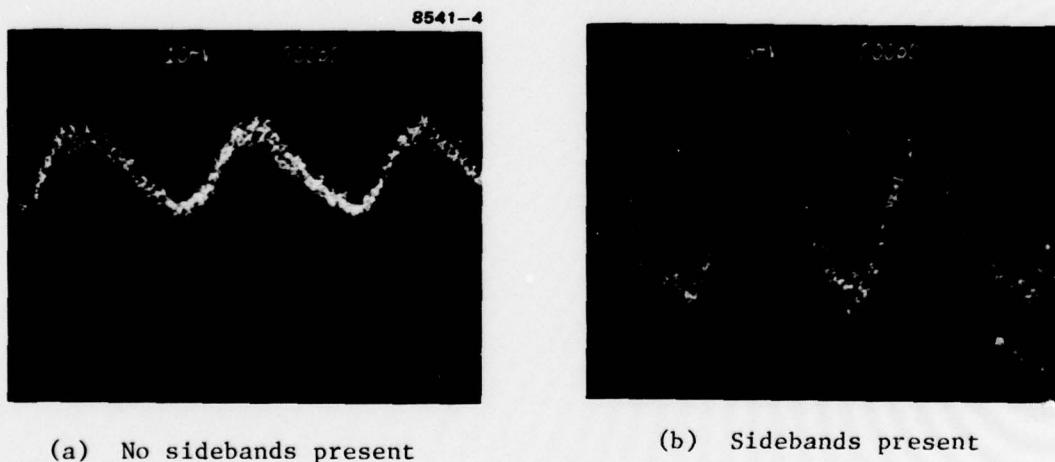
Figure 7. Laser output pulse shape under two different conditions (positive going pulses).

8541-6

(a) Without external rf drive   (b) With rf drive
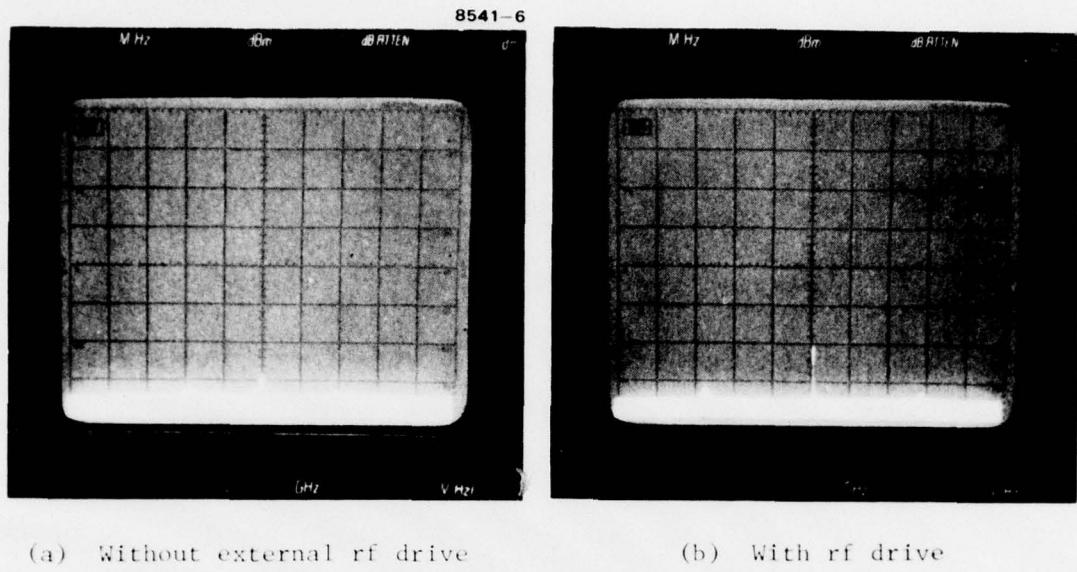
Figure 8. Microwave spectrum of laser output.

8541-7
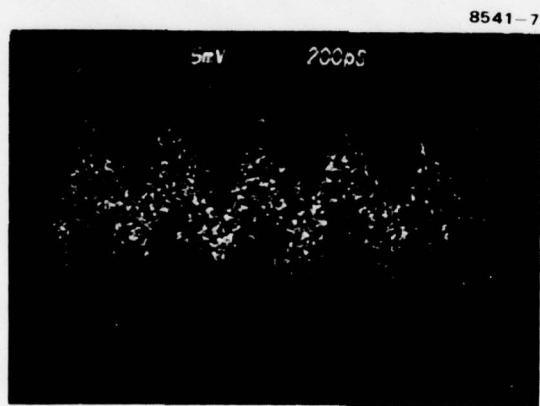
Figure 9.
Laser output shape when driven at
2.82 GHz (positive going pulses).

evidence that the magnitude of the low-frequency resonance is related to the sharpness of the laser output pulses. To further emphasize the importance of perfect alignment, Figure 10 shows the effect of cavity alignment on the laser output pulse shape.

We have also carried out experiments using stripe geometry lasers from RCA. These lasers have a threshold current of about 80 mA and display no kinks in their light output versus driving current curve. When the cavity was aligned with the laser, a resonance at a frequency of approximately 2.9 to 3.0 GHz was observed. In Figure 11, the amplitude of the resonance is plotted versus driving current for both the RCA laser and the Laser Diode laser without external rf signal. The RCA laser displays a resonant behavior, while in the LCW-10 diode the amplitude of the resonance increases monotonically. The RCA laser shows no low-frequency resonance (self-pulsation), and therefore no sidebands are observed around the cavity transit frequency resonance. When an rf signal is applied to the laser, the output modulation is primarily sinusoidal. The second harmonic content of the optical output signal (at 6 GHz) is ~20 dB below the fundamental component. We believe that there is little or no mode locking taking place in this case, which would reinforce the notion that laser self-pulsation is essential to the generation of sharp pulses.

D.   FREQUENCY RESPONSE OF INJECTION LASERS WITH OPTICAL FIBER RESONATOR

The use of an external cavity in conjunction with a semiconductor laser can provide a convenient way of mode locking an injection laser at gigahertz rates. Previous experiments used a spherical mirror as shown in Figure 1. Cavity alignment was achieved using precision translation stages. To realize a practical system requires a mechanically rugged assembly. One promising method we tried is to replace the external mirror by a piece of optical fiber. One end of the fiber was coated with a thin layer of gold to form a reflector. The other end was heated to form a spherical lens for better laser-to-fiber

23

TILTING MIRROR

ALIGNED MIRROR
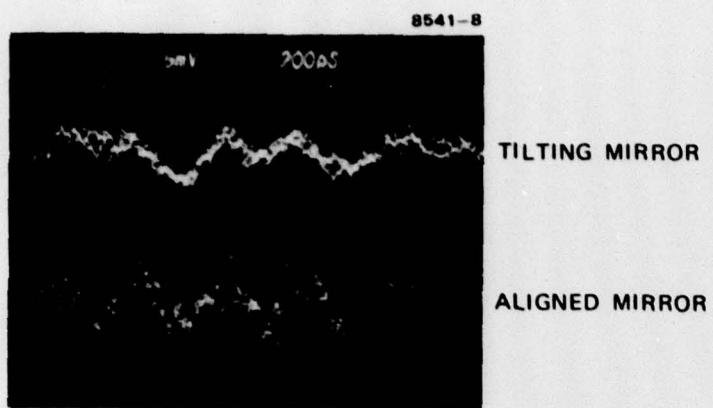
Figure 10.
Effect of cavity alignment on the output
pulse shape of an injection laser (posi-
tive going pulses).
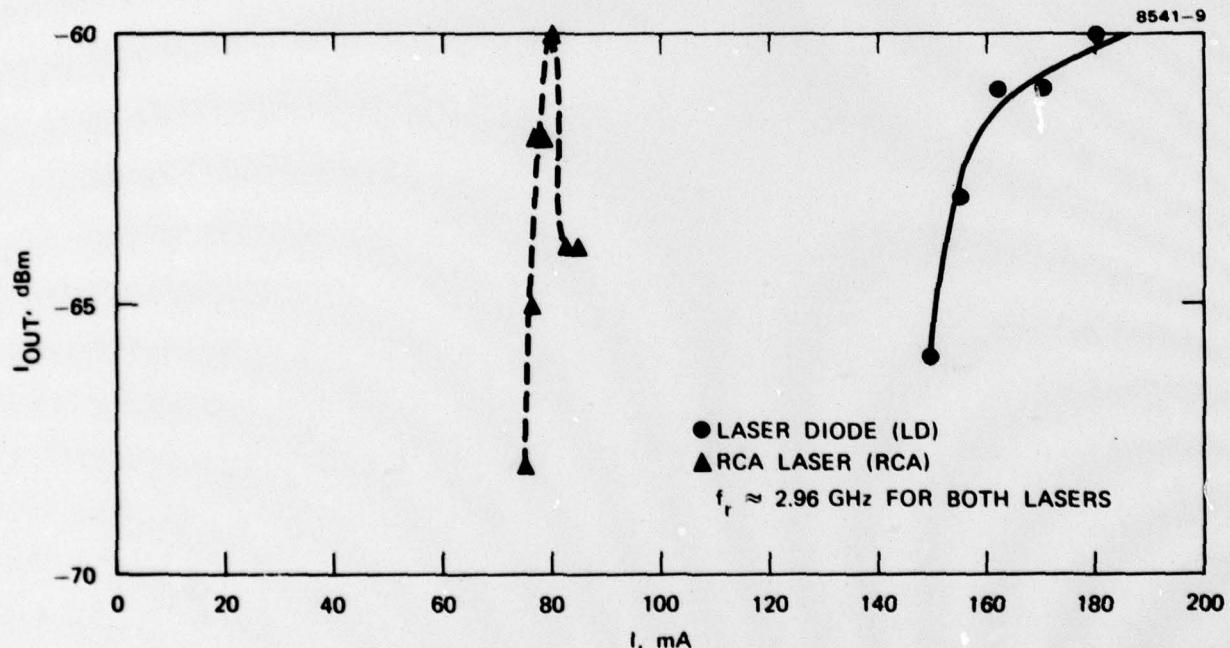
Figure 11. Amplitude of laser cavity resonance versus driving current of two
different laser diodes.

coupling efficiency. Figure 12 is a plot of the resonant frequency of the fiber resonator as observed on a spectrum analyzer versus the fiber length. The resonant frequency f_R is given by

$$f_R = \frac{c_o}{2L\,n_c} \quad ,$$

where c_o is the speed of light in vacuum, L is the fiber length, and n_c is the index of refraction of the fiber guide. Figure 12 shows that n_c is equal to 1.534. A typical resonant frequency spectrum is shown in Figure 13(a). The width of the resonance is $\sim$50 MHz without rf driving signal. Once the rf signal is applied to the laser, the frequency component at 2.3 GHz of the laser output narrows to roughly the width of the signal source. Figure 13(b) is the temporal display of the laser output driven by an rf signal at 2.3 GHz. Figure 13(c) is obtained when the driving signal is at 1.15 GHz. The outputs show pulsation behavior, and the pulse width is on the order of 150 psec. Interestingly, the laser can be driven at one-half the transit time frequency ($f_c/2$) and still give output pulses at the transiet time frequency (f_c). As the drive frequency approaches $f_c/2$, the amplitudes of the components at f_c and $2f_c$ increase while that of the component at $f_c/2$ decreases. This effect has been observed in all the lasers tested and in resonators with various lengths. Figure 14 shows the temporal display of laser output using a 13.2-cm-long fiber resonator. The transit time frequency in this case is 0.74 GHz. Since the fiber in Figure 14(a) was not aligned, the output pulse had long rise and fall times. Figure 14(b) shows the case when the fiber resonator was aligned with the laser. Significant narrowing of the pulse is seen in addition to the added substructures within the pulse. Because of the frequency response limit of our photodiode, we were not able to resolve the substructures of the pulse output, which we suspect is where the true mode-locked pulse lies.

In the next quarter, we will be setting up an autocorrelation measurement apparatus so that we can measure the true width of mode-locked laser pulses.

25
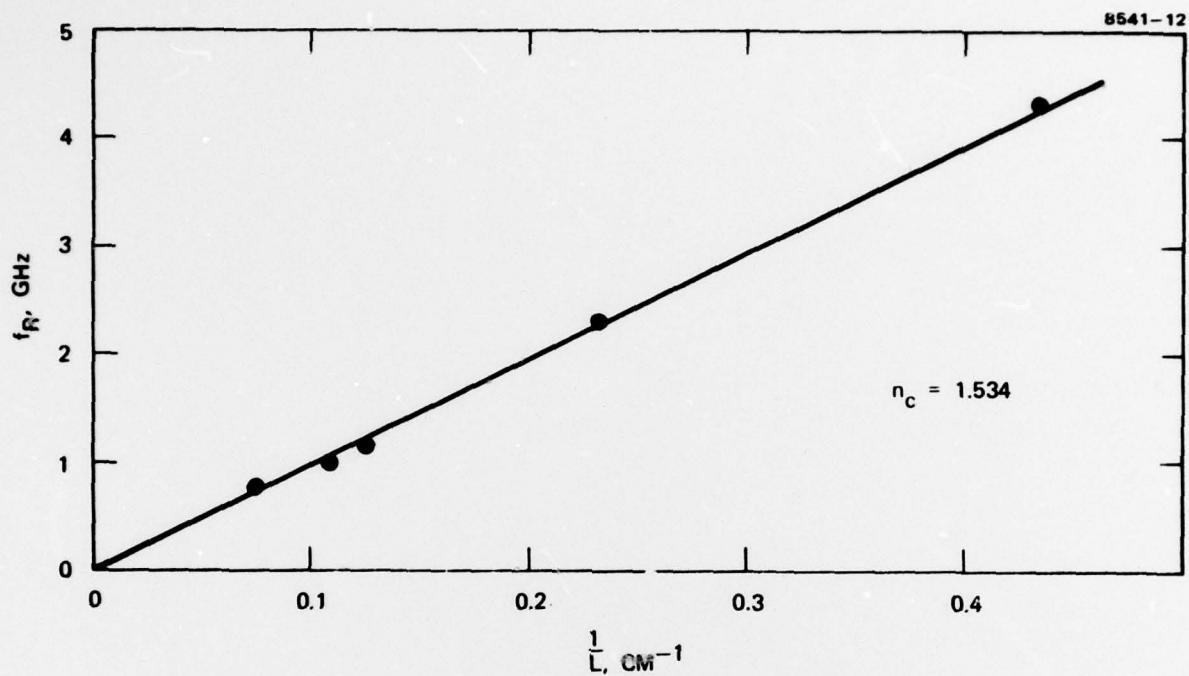
Figure 12. Cavity resonance frequency versus fiber length of an injection laser with external fiber resonator.
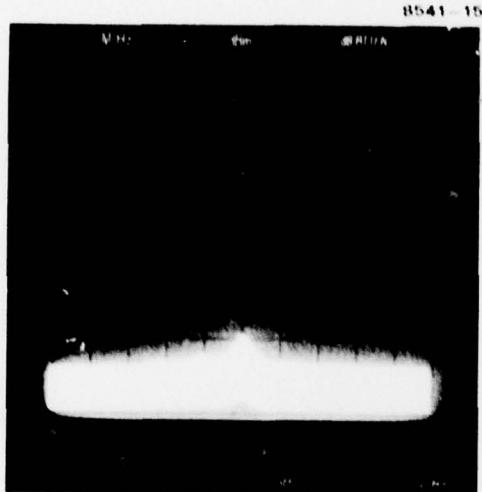
(a) Cavity resonance at 2.3 GHz.
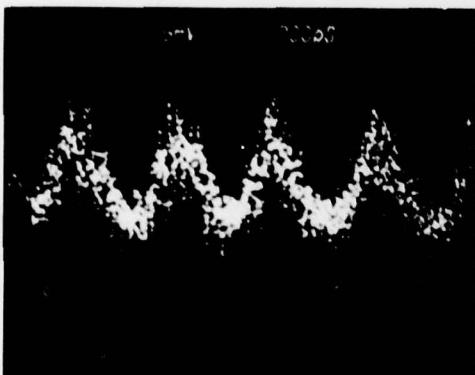
(b) Pulse shape when driven at
2.3 GHz (positive going).
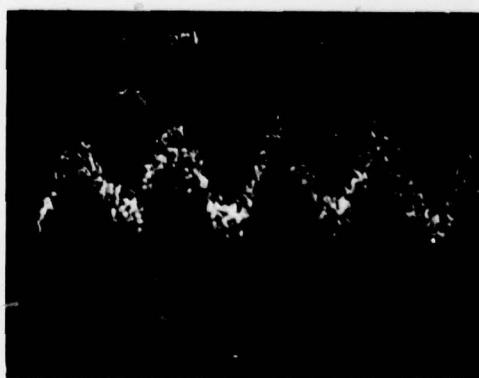
(c) Pulse shape when driven at
1.15 GHz (positive going).

Figure 13. Microwave spectrum and pulse shape of an injection laser
operating in an optical fiber resonator.
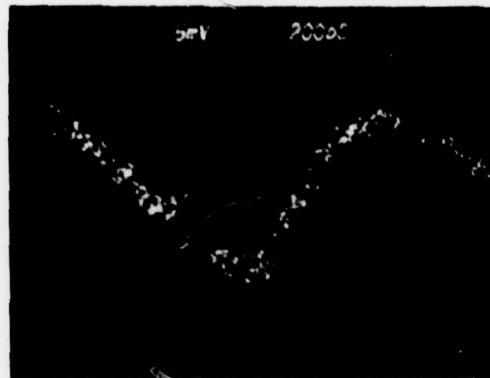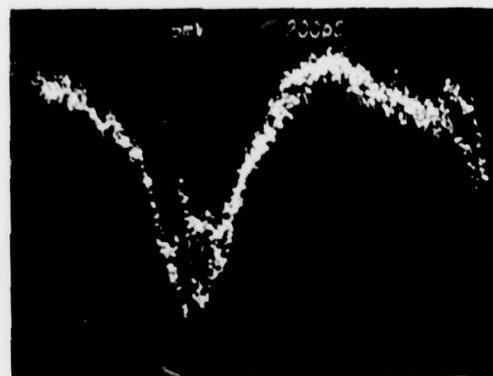
a) NO ALIGNMENT

b) ALIGNMENT

Figure 14.
Output pulse shape of a laser in
fiber resonator (negative going).

SECTION 3

DESIGN CONSIDERATIONS OF A PHOTO-FET

The generation of electron-hole pairs in a semiconductor under optical illumination can be used to design a light-sensitive FET. The GaAs MESFET is presently the highest frequency transistor, so it can be used with high-speed modulated light. Excess carrier generation under illumination can change (1) the resistance of the various regions of the MESFET and (2) the depletion region under the gate.

The change in the depletion thickness can be due to excess carrier generation in the depletion region or to a change in the gate voltage brought about by the gate photocurrent. The former effect is negligible. This can be shown from Poisson's equation for a p-n junction:

$$\frac{-\partial^2 V}{\partial x^2} = \frac{q}{\epsilon} \{ p(x) - n(x) + N_D^+(x) - N_A^-(x) \} . \tag{7}$$

The depletion region extends from $-x_p$ on the p side to x_n on the n side. For an n-type Schottky barrier, we assume $x_p = 0$ and just treat the n side. In the depletion region,

$$\frac{-\partial^2 V}{\partial x^2} = \frac{q}{\epsilon} \{ N_D^+ \} \tag{8}$$

for a uniform doping. Under illumination, the free carrier distribution changes from the equilibrium levels (i.e., no illumination) of $n_o(x)$ and $p_o(x)$ to the new levels of $n_o(x) + \delta_n(x)$ and $p_o(x) + \delta_p(x)$, respectively. Since $n_o(x)$, $p_o(x) \ll N_D^+$ in the depletion region, Eq. 8 becomes

$$\frac{-\partial^2 V}{\partial x^2} = \frac{q}{\epsilon} [\delta_p(x) - \delta_n(x) + N_D^+] . \tag{9}$$

Thus, the excess carrier generation has the effect of changing the background space charge in the depletion region. If we assume the electrons and holes are swept out of the depletion region at drift velocities

29

v_n and v_p, respectively, and ignore recombination, then the excess carrier densities are

$$\delta_n(x) = \eta \frac{P_{inc}}{h\nu} \frac{1}{v_n} \tag{10a}$$

$$\delta_p(x) = \eta \frac{P_{inc}}{h\nu} \frac{1}{v_p} \;, \tag{10b}$$

where P_{inc} is the optical power density incident on the semiconductor, $h\nu$ is the photon energy, and η is the quantum efficiency (including reflection losses). This assumes a uniform (rather than exponential) spatial generation rate and will serve to display the magnitude of the essential physical processes.

Under illumination, the Poisson's equation can therefore be written as

$$\frac{-\partial^2 V}{\partial x^2} = \frac{q}{\varepsilon} \left\{ \eta \frac{P_{inc}}{h\nu} \left(\frac{1}{v_p} - \frac{1}{v_n} \right) + N_D^+ \right\} . \tag{11}$$

Under high fields ($E \gtrsim 10^5$ V/cm), the drift velocities of holes and electrons saturate at the same value, $\sim 8 \times 10^6$ cm/sec.[12] Thus, for large gate voltages, the electrons and holes will be swept out of the depletion region at the same rate, and there will be no change in the depletion width. At lower fields, $E \sim 10^4$ V/cm, $v_p \sim 2 \times 10^6$ cm/sec, $v_n \sim 10^7$ cm/sec, and therefore

$$\delta_p - \delta_n = \left(\eta \frac{P_{inc}}{h\nu} \right) (4 \times 10^{-5}) \;, \tag{12}$$

where all quantities are in MKS units. Typical doping densities are $\sim 10^{17}/\text{cm}^3 = 10^{23}/\text{m}^3$. For $h\nu = 1.6 \times 10^{-19}$ J = 1 eV, $\eta \sim 1$, and $P_{inc} = 1$ mW$/(10 \ \mu\text{m})^2 = 10^7$ W/m^2, we find that

$$\delta_p - \delta_n \sim 2.5 \times 10^{21}/\text{m}^3 \;.$$

30

Thus, with a power density of 10^{-2} mW/μm^2, the excess carrier distribution is negligible compared with the background doping. However, if the same power density illuminated a gate region of $\sim 1 \times 100$ μm^2, the gate photo-current would be ~ 1 mA. If the gate were loaded with 50 Ω, the change in gate voltage would be ~ 0.05 V, which would strongly influence the depletion width.

It appears reasonable to assume that the change in the depletion region under the gate due to illumination is caused by a change in the gate voltage. The equivalent circuit of the MESFET under illumination (Figure 15) will contain only added current source terms due to excess carrier generation. The transconductance g_m will only be dependent on illumination when the intensity is great enough to affect the depletion region by excess carrier generation. We will assume that g_m is a constant.

The substrate leakage resistance and photocurrent can be eliminated by fabricating the MESFET on an undoped $Ga_{1-x}Al_xAs$ substrate that will be insulating and transparent to the illumination ($h\nu \sim E_g$). Figure 16 shows the photocurrents schematically. The current sources are defined as follows: i_{ch} is the added current flowing through the channel due to illumination, i_{gs} and i_{gd} are the photocurrents flowing through the Schottky-barrier gate. The substrate photocurrent, i_{sub}, will be ignored. The magnitude of each of the photocurrents will depend on the mode of illumination (top, bottom, or edge) and the field distribution in the MESFET.

The MESFET can be operated in two basic modes. In the first, it is operated as a simple photoconductor where carrier generation between the source and drain gives rise to a channel current.[13,14] The gate can be used to adjust the impedance of the photoconductor. In the second, it is operated as a phototransistor where i_{gs} and i_{gd} induce a change in the gate voltage, ΔV_g. This in turn causes a change in the source-drain current

$$i_{ds} = g_m \Delta V_g \ .$$

(13)

31
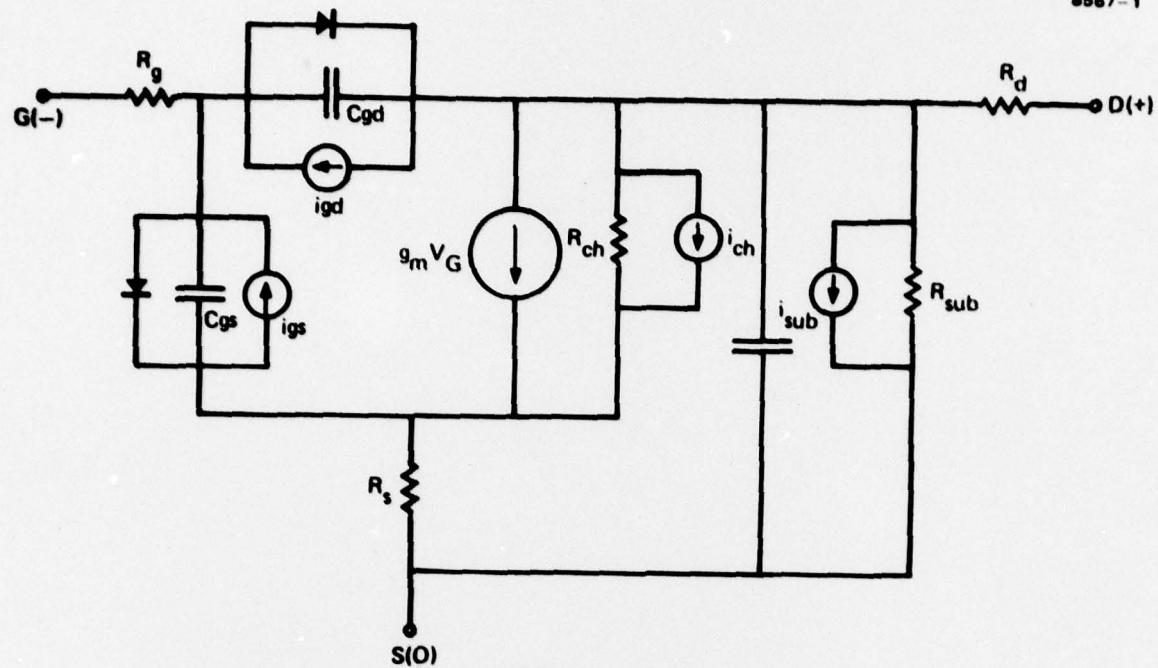
Figure 15. Equivalent circuit of an FET under optical illumination.
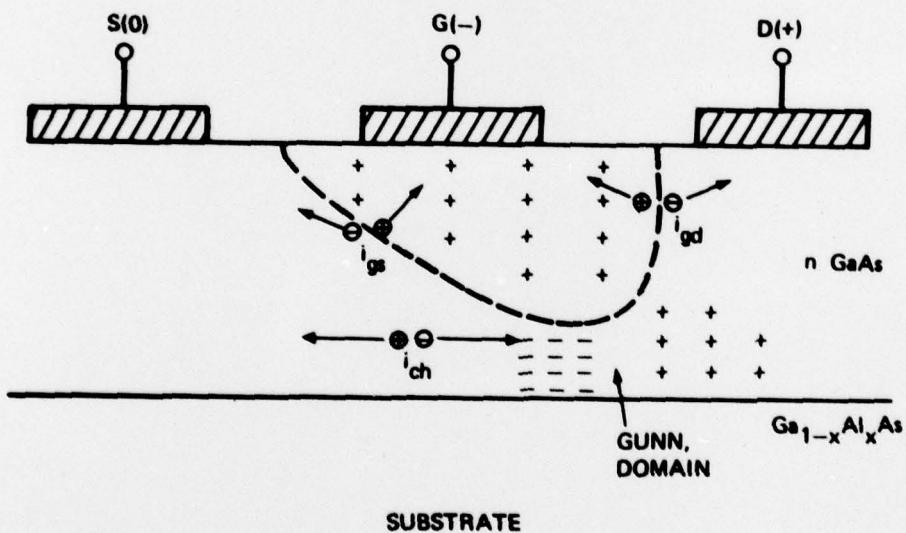
Figure 16. Schematic of photocurrent generation process inside an FET.

32

Pan[15] has observed a change in the depletion layer capacitance under illumination. This is presumably due to the change in the gate voltage. However, no observations of photo-transistor action have been reported. Baack et al.[13] and Gammel et al.[14] have both observed source-drain photo-current beyond the pinchoff voltage, indicating photoconductive operation.

To obtain photo-transistor operation, which has many more interesting applications than does simple photoconductor operation, it appears that the gate region must be more fully illuminated. Past experiments[13-15] have covered only top illumination, where the gate region is shadowed by its own metalization. Only the edge of the gate-source and gate-drain regions were illuminated. With edge or bottom illumination, it appears that the gate will play a more active role in the operation of the MESFET, making it a promising candidate for a high-frequency phototransistor.

To achieve optical injection locking, mixing, and high-speed detection using GaAs FET amplifiers or oscillaotrs, we are interested in improving the optical coupling efficiency of GaAs FETs. Figure 17(a) shows the conventional GaAs FET structure. Top illumination has been used to couple light into such a structure. The disadvantage of this approach is the small active area available for optical absorption due to the presence of the gate electrode.

To enhance the efficiency of optical coupling, we have previously proposed a modified device structure by incorporating an optical wave-guide into FETs, as shown in Figure 17(b). Instead of having the n-GaAs channel layer grown directly on the GaAs semi-insulating substrate, an undoped $Ga_{1-x}Al_xAs$ layer is grown in between. This makes the n-GaAs channel layer an optical waveguide since the index of refraction of $Ga_{1-x}Al_xAs$ is lower than that of the GaAs layer. By edge illumination, one would expect the optical energy to be trapped in the channel layer and generate carriers across the length of the channel layer. The penetration depth of the optical signal depends on the radiation wavelength. For strong absorption, a small and highly conductive region near one end of the FET is created while the rest of the device is left unaltered.

33
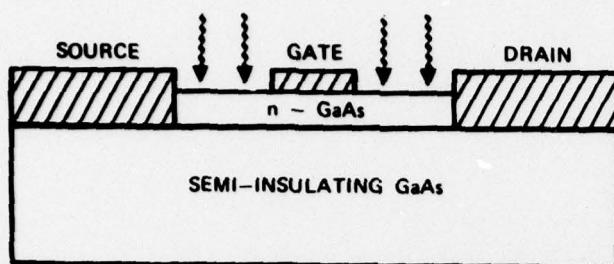
(a) Conventional
    structure with
    top illumination.
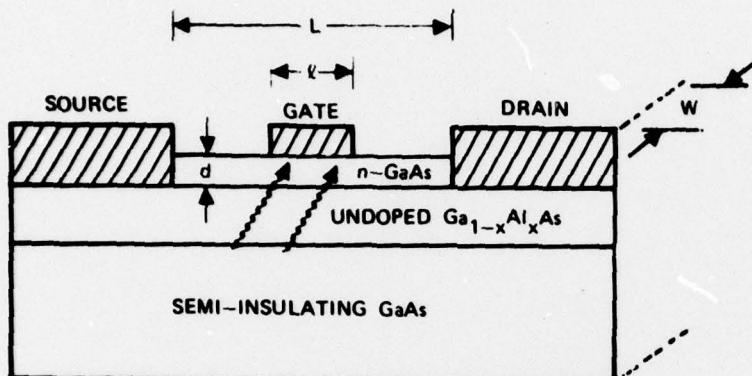
(b) Modified struc-
    ture with edge
    illumination.
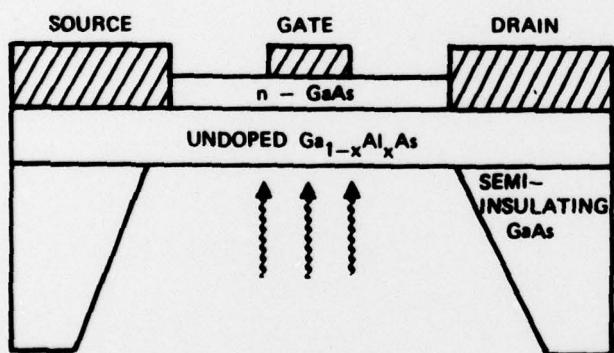
(c) Improved
    structure with
    back illumination.

L = CHANNEL LENGTH
ℓ = GATE LENGTH
w = GATE WIDTH
d = CHANNEL THICKNESS

Figure 17. GaAs FET structures for optical illumination.

34

For weak absorption, the penetration depth increases and the generated photocarriers are more uniformly distributed. In both cases, though, the incident optical power can be absorbed completely in the channel layer (since the channel width is typically a few hundred micrometers). The effect of nonuniform illumination is not yet clear; however, as far as photoconductivity is concerned, this is a good approach. The disadvantage of this structure is that it requires precise optical beam focusing since the channel thickness is only about 1 μm. Also, the FET edge should be accessible for input optical coupling; surface recombination may reduce the optical detection efficiency.

A recently conceived device is shown in Figure 17(c) where a Burrus-type structure is used for the FET. In this new structure, the $Ga_{1-x}Al_xAs$ layer serves several functions: (1) serves as an optical window, transparent for photon energy lower than the $Ga_{1-x}Al_xAs$ bandgap energy; (2) reduces GaAs surface recombination loss; (3) provides mechanical support; and (4) serves as the stop for the selective etching process during fabrication. The main advantages of this structure are that the whole channel layer can be uniformly illuminated and the active area is large because the gate electrode is out of the way. We do not feel that the added $Ga_{1-x}Al_xAs$ layer will have any significant adverse effect on the FET's operation. The $Ga_{1-x}Al_xAs$ layer is essentially a buffer layer. By not doping the layer, we can keep its conductivity low. By choosing an appropriate percentage of Al such that $Ga_{1-x}Al_xAs$ becomes an indirect gap material, we can further reduce the carrier mobility in this layer. Since the bandgap energy of $Ga_{1-x}Al_xAs$ is higher than that of GaAs, the heterojunction also serves to confine charge carriers in the GaAs channel layer. Thus, the current leakage due to the presence of the $Ga_{1-x}Al_xAs$ layer will be minimum. The only tradeoff involved in substituting this structure is added complexity in fabrication.

SECTION 4

PLANS FOR THE NEXT QUARTER

In the next quarter we will continue the injection laser mode-locking experiment. Emphasis will be on the determination of the actual laser output pulsewidth. An optical intensity correlator using phase-matched second-harmonic generation in a nonlinear crystal will be set up for this purpose.

GaAs FETs have been found to be promising high-speed photodetectors. To increase their sensitivity and obtain possible phototransistor action, the active surface of the device must include the region under the gate electrode. During the next quarter we will attempt to fabricate Burrus-type photo-FETs. Both conventional photolithography and E-beam lithography will be used to fabricate a whole range of devices with various dimensions. These new devices will be tested not only for high-speed optical detection efficiency but also in terms of microwave oscillator injection-locking performance.

REFERENCES

1. F. Stern, IEEE J. Quantum Electron., 9, 290 (1973).

2. K. Aiki, M. Nakamura, T. Kurada, and J. Umeda, Appl. Phys. Lett. 48, 649 (1977).

3. L. Figueroa and S. Wang, Appl. Phys. Lett. 32, 55 (1978).

4. D. Kato, J. Appl. Phys. 44, 2756 (1973).

5. T. Ikegami and Y. Suematsu, IEEE J. Quantum Electron. 4, 149 (1968).

6. H.W. Yen and M.K. Barnoski, Final Report, Contract N00173-77-C-0156, July (1978).

7. R.F. Broom, E. Mohn, C. Risch, and R. Salathe, IEEE J. Quantum Electron. 6, 328 (1970).

8. T.L. Paoli and J.E. Ripper, Appl. Phys. Lett. 15, 105 (1969).

9. T.L. Paoli and J.E. Ripper, Phys. Rev. Lett. 22, 1085 (1969).

10. J.E. Ripper and T.L. Paoli, Appl. Phys. Lett. 18, 466 (1971).

11. T.L. Paoli and J.E. Ripper, IEEE J. Quantum, Electron. 6, 335 (1970).

12. S.M. Sze and R.M. Ryder, Proc. IEEE 59, 1140 (1971).

13. C. Baack, G. Elze and G. Walf, Electronics Lett. 13, 193 (1977).

14. J.C. Gammel and J.M. Ballantyne, IEDM Technical Digest, 120 (1978).

15. J.J. Pan, 22nd SPIE Int. Tech. Symp., San Diego, Aug. 1978.